MARS GLOBAL SURVEYOR
Ka-BAND FREQUENCY DATA ANALYSIS

D. Morabito, S. Butman, and S. Shambayati
Jet Propulsion Laboratory
California Institute of Technology
4800 Oak Grove Dr. 161-260
Pasadena, California 91109
USA
Phone: 818-354-2424, Fax: 818-393-4643, E-mail: ddm@godzilla.jpl.nasa.gov

1. ABSTRACT

The Mars Global Surveyor (MGS) spacecraft, launched on November 7, 1996, carries an experimental space-to-ground telecommunications link at Ka-band (32 GHz) along with the primary X-band (8.4 GHz) downlink, used for operational MGS Project activities. The signals are simultaneously transmitted from a 1.5-m diameter parabolic antenna on MGS and received by a beam-waveguide (BWG) R&D 34-meter antenna located in NASA's Goldstone Deep Space Network (DSN) complex near Barstow, California. The two signals have been routinely tracked between December 1996 and December 1998. Carrier signal-level data results demonstrating the advantage of Ka-band over X-band were presented in previous articles. Analysis of frequency (f_x and f_{Ka}) and difference frequency (f_x-f_{Ka} /3.8) data from the experiment are presented in this article. The measured frequencies and residuals were found to agree between bands and have statistics consistent with those of expected noise sources.

2. INTRODUCTION

The use of Ka-band (32 GHz) as a telecommunications link frequency is predicted to add about 5 dB advantage in gain over that of X-band (8.4 GHz), the primary deep-space telecommunications link frequency of today. This link advantage was demonstrated using the signal strength data acquired from the first two years of the Mars Global Surveyor (MGS) Ka-band link experiment (MGS/KaBLE-II) as well as successfully conducting end-to-end telemetry and ranging demonstrations [1-3]. In addition to carrier signal level data, the MGS/KaBLE-II experiment also produced carrier phase and frequency data. This article will focus on the analysis of the frequency data acquired during the link experiment. The spacecraft and station configurations will first be briefly described as they pertain to the frequency data. The reader is referred to the references [1-3] for additional detail.

3. SPACECRAFT CONFIGURATION

The Ka-band downlink signal is derived from a sample of the X-band downlink signal which is upconverted to 32 GHz, amplified and radiated from a dual-frequency (X/Ka) High Gain Antenna (HGA). The upconverter first downconverts the X-band sample at 8.42 GHz to a frequency of 8 GHz which is then multiplied by a X4 multiplier producing the 32 GHz Ka-band frequency. During the first two years of tracking of the link experiment, the Ka-band frequency was either coherent with the X-band downlink or a hybrid combination of USO (Ultra Stable Oscillator) and VCO (Voltage Controlled Oscillator) derived frequencies depending upon the X-band uplink status and the programmed setting of a switch on-board the spacecraft. The Ka-band downlink signal is coherent with the X-band downlink signal when the downconverter is driven by the same frequency source as the X-band signal. The Ka-band data presented in this article are coherent with the X-band data, that is both signals have the same frequency reference source. The Ka-band frequency, f_{Ka}, is thus an exact factor of 3.8 that of the X-band frequency, f_X ($f_{Ka} = 3.8\ f_X$).

4. GROUND SYSTEM CONFIGURATION

The ground station used to acquire the data is DSS-13, a 34-meter beam-waveguide (BWG) antenna located at the NASA Goldstone Deep Space Tracking Complex near Barstow, California. This antenna incorporates a series of mirrors inside beam waveguide tubes which guide and focus the RF energy onto feed horns on low noise amplifiers (LNA) residing in a subterranean pedestal room. A dichroic plate allows simultaneous reception of both X-band and Ka-band signals. The LNA output RF signals are downconverted to IF near 300 MHz, and transported via optical fiber to a control room where they are input to the various receivers.

The Experimental Tone Tracker (ETT) is a digital phase-lock-loop (PLL) receiver which was used to simultaneous track both X-band and Ka-band carrier signals during the tracks. The analog IF signal input to the ETT are open-loop downconverted to baseband and then digitized. Once a signal is detected, the ETT's digital PLL's extract estimates of the carrier SNR (Pc/No) in a 1-Hz bandwidth as well as phase and frequency at baseband. These data are written at 1-second intervals onto output data files for later processing.

5. RESULTS

This section describes the results of the analysis performed on X-band and Ka-band frequency data acquired from MGS between January 1997 and December 1998. All Ka-band data used in the analysis were coherent with the X-band data. The following frequency data analysis results will be discussed; individual band frequency residuals for Ka-band and X-band, differenced X/Ka data with emphasis on Allan deviation results, and one-way USO-referenced Ka-band and X-band frequency estimates.

5.1 Frequency Residuals

The ETT produced phase and frequency data for passes conducted between January 1997 to December 1998. During several of these passes, the downlink carrier reference was either the on-board USO (one-way mode), or a transponded version of an X-band uplink signal generated by an operational DSN station during normal operations through the spacecraft's VCO (three-way mode). The Ka-band downlink frequencies for these passes are coherent with the X-band downlink frequencies (multiplier of 3.8).

The estimates of received baseband phase at 1-second sampled time tags from the station generated ETT data files are converted to received sky frequency estimates by post-experiment software and written onto output files. These files containing time tags and received sky frequencies were input to the STBLTY analysis program set [4] developed for Radio Science. STBLTY produces frequency residuals, Allan deviation, reconstructed phase, frequency and phase power-density, and estimates of the frequency emitted at the spacecraft (USO frequency when data are one-way). Frequency residuals for the individual bands were computed by removing a model frequency (including Doppler) from each observable frequency at each time tag. A simple troposphere correction was applied to the data. No ionosphere correction was applied. The model frequency was estimated from MGS Navigation Team trajectory files.

The first pass after the HGA was fixed on earth point while the spacecraft radiated both X-band and Ka-band signals occurred on January 17, 1997. The frequency residuals for individual bands for this pass are displayed in Figure 1a (X-band residuals) and Figure 1b (Ka-band residuals). The linear trends are attributed to the aging behavior of the USO (0.23 Hz/day at X-band) and the systematic sinusoidal signatures are attributed to dynamic motion of the spacecraft which is not modeled in the trajectory (spacecraft spin).

Table 1 summarizes the Allan deviations, $\sigma_y(\tau)$ at $\tau = 1, 10, 100$ and 1000 sec for the individual-band X-band and Ka-band frequency residuals of the January 17, 1997 pass. Also in Table 1, for comparison, are the pre-flight USO Allan deviation measurements which agree with the individual band values when other effects do not dominate, and the Allan deviation of the difference of the X-band and Ka-band frequencies, (f_x - f_{Ka}/3.8).

The X-band and Ka-band Allan deviations are in good agreement with each other for all time intervals τ = 1, 10, 100 and 1000 sec. The individual band Allan deviations agree with the USO preflight value at 1 sec, but are somewhat higher than the USO preflight value at 10 and 100 sec, and are significantly higher than the USO preflight value at 1000 sec. The higher Allan deviations at 10 and 100 sec may include contributions from sources other than the USO, such as troposphere and unmodeled spacecraft motion. The 1000 sec Allan deviation values are believed to be dominated by a combination of USO aging (which has been removed in the preflight data), and unmodeled spacecraft motion. When the sinusoidal and aging trends are removed from the residuals, the DSS-13 X-band and Ka-band $\sigma_y(\tau$ = 1000-s) reduce to 1.2×10^{-13}. This value is nearer the pre-flight value of 0.97×10^{-13}. The 1-second Allan deviations are dominated by the USO as they agree closely with its pre-flight value (1.3×10^{-13}). Thus, the frequency residuals estimated for individual frequency bands for this pass are dominated by the USO (when in the one-way mode) and unmodeled dynamic spacecraft motion in the form of significant trends.

For passes where Ka-band is coherent with X-band, the received downlink Ka-band frequency is an exact factor of 3.8 times the X-band received frequency. By taking frequency differences across identical time tags of the form f_x-f_{Ka}/3.8, all non-dispersive error contributions, including unmodeled dynamic spacecraft motion, USO aging and troposphere, cancel out in the resulting residuals. The remaining noise sources should include thermal noise (significant at small time scales) and charged particles (which dominate at higher time scales). The difference frequency residuals are effectively a measure of the charged particle effect on the X-band link since the effect at Ka-band is significantly smaller (by the ratio of the frequencies squared). The resulting frequency differences in Figure 1c for the January 17, 1997 data clearly display a significantly cleaned and flattened residual plot.. The corresponding Allan deviation versus time interval plot of these frequency differences is displayed in Figure 1d.

The troposphere contributes noise to the individual band Allan deviations. However, this contribution cancels out in the difference frequency and thus its effect is removed in the difference frequency Allan deviations along with all other non-dispersive noise sources. The X-band and Ka-band carrier signal strengths were comparable during January 17, 1997 (X-band Pc/No=56 dB-Hz, Ka-band Pc/No=53 dB-Hz). The difference frequency Allan deviations for 10, 100, and 1000 seconds significantly exceed predictions based on thermal noise estimates derived from the Pc/No data, and are thus attributed to charged particle effects on the X-band link.

Table 1

Allan Deviation Summary for January 17, 1997 Data

τ (sec)	X-band $\sigma_y(\tau)$	Ka-band $\sigma_y(\tau)$	USO Pre-flight[1] $\sigma_y(\tau)$	(f_x - f_{Ka}/3.8)/f_x $\sigma_y(\tau)$
1	1.15×10^{-13}	1.11×10^{-13}	1.34×10^{-13}	0.36×10^{-13}
10	1.01×10^{-13}	1.00×10^{-13}	0.64×10^{-13}	0.12×10^{-13}
100	0.96×10^{-13}	0.97×10^{-13}	0.72×10^{-13}	0.06×10^{-13}
1000	3.91×10^{-13}	3.93×10^{-13}	0.97×10^{-13}	0.09×10^{-13}

For most of the other passes conducted throughout the two-year period, thermal noise dominated the lower time intervals (1-sec and 10-sec) of the individual X-band and Ka-band residuals as the spacecraft range increased and the carrier SNR decreased. Allan deviations at 100-s were consistent with media or the USO for most passes as thermal noise did not appear

[1] "Final USO Test Results" conducted at JPL Frequency Standard Test Laboratory by Al Kirk, Test Engineer, on August 18-21, 1995.

to dominate at that time scale. Single-band Allan deviations at 1000-s were dominated by unmodeled dynamic motion of the spacecraft and the USO.

For those passes in which significant durations of simultaneous coherent X-band and Ka-band data were acquired, the Allan deviations of the difference data type (f_x-f_{Ka}/3.8) were estimated. Figures 2a-d display these Allan deviations versus day number for time intervals of 1-sec, 10-sec, 100-sec and 1000-sec, respectively. The "+" symbols on Figures 2a-d denote actual measurements and the "*" symbols denote estimates based on thermal noise (computed from Pc/No measurements). The Allan deviation for the short time intervals were generally in agreement with the predictions based on thermal noise for most passes, where other effects such as charged particles did not dominate. The significant increase in Allan deviation between days 485 and 515 on Figures 2a-d is due to charged particles during the May 1998 solar conjunction period when the spacecraft signal ray path passed near the sun.

The 1000-s Allan deviations are displayed in Figure 3 as a function of solar elongation angle. A general trend is apparent which shows Allan deviation decreasing as solar elongation angle increases from near 6° to about 170°. This trend is consistent with a model curve derived from S-band Viking data acquired between 1976 and 1978 [5]. The expected thermal noise contributions to the 1000-s Allan deviations lie well below the observed Allan deviations as shown. The majority of the 1000-s Allan deviations in Figure 3 clustered at high solar elongation angles (above 160°) are in good agreement with a predicted Allan deviation of $6x10^{-15}$ for the anti-solar direction at X-band [5]. The Ka-band data are thus useful for removing all non-dispersive error sources from the X-band data thus allowing solar plasma effects to be probed.

5.2 One-way USO-Referenced Frequency Data

Figure 4 displays the USO frequencies estimated from the DSS-13 ETT X-band and Ka-band data (X and K symbols) using STBLTY as well as independent X-band data acquired at operational DSN stations during MGS Radio Science USO experiments[2] (S symbols). A few X-band only DSS-13 passes were included in cases where insufficient Ka-band data were acquired or Ka-band was configured in the hybrid mode. Evident upon inspection of Figure 4 is the increasing aging trend of the USO which is about 0.23 Hz/day. The uncertainties of the individual pass USO frequencies for DSS-13 and MGS Radio Science X-band generally run from about 2 mHz to 10 mHz, while for DSS-13 Ka-band, they range from 10 mHz to 60 mHz. (for one-second sampled data over typical experiment durations of one to several hours).

When the DSS-13 data are compared against the independently acquired and processed Radio Science data, the individual experiment USO frequencies are found to agree within 1 Hz. Figure 5 displays the differences of the individual USO frequency estimates of Figure 4 with a quadratic fit of the MGS Radio Science X-band USO data. The DSS-13 X-band and Ka-band data are biased about 0.2 Hz above the fitted model of the MGS Radio Science data. The linear trend of the DSS-13 residuals in Figure 5 between day number 160 and 200 appears to be the source of a significant amount of this small discrepancy, but its cause has not been identified nor its statistical significance quantified. The sub-Hz differences between the Radio Science and the DSS-13 USO frequencies are attributed to different models and software algorithms, different stations and equipment, and statistical effects of using different data intervals.

Table 2 is a summary of the residuals of quadratic fits over each data set. There is good agreement between all three data sets with the MGS Radio Science data set having the least amount of RMS residual scatter (0.16 Hz versus 0.3 Hz) about its quadratic fit.

[2] MGS Radio Science Team; D. Hinson and J. Twicken, Stanford University.

Figure 6 displays the differences of the individual pass DSS-13 X-band USO frequency and DSS-13 Ka-band USO frequency (divided by 3.8) determined over common data spans. The DSS-13 X-band and Ka-band USO frequency estimates over common data periods were all within 10 mHz of each other. The average of the $f_X(uso)$ - $f_{Ka}(uso)/3.8$ differences plotted in Figure 6 was -0.7 mHz with an rms scatter of 2 mHz.

Table 2
USO Fit Analysis Results
(Referenced to X-band)

Data Set	RMS (Hz)	Slope Term (Hz/Day)	Offset Frequency (Hz)	Number of Passes
X-band (DSS-13)	0.296	0.2291 ± 0.0009	8423152938.662 ± 0.09	33
Ka-band (DSS-13)	0.311	0.2290 ± 0.0010	8423152938.822 ± 0.13	23
X-band (Radio Science)	0.163	0.2266 ± 0.0008	8423152938.479 ± 0.08	19

6. CONCLUSION

The MGS/KaBLE-II link experiment measured frequency residuals which were in agreement between bands and whose statistics were consistent with expected noise sources. The DSS-13 X-band and Ka-band USO frequencies estimated from common time periods agreed between bands to better than 10 mHz, and these estimates agreed with independent MGS Radio Science estimates to better than 1 Hz.

7. ACKNOWLEDGMENTS

We would like to thank J. Armstrong, J. Layland, and R. Woo of JPL, and W. Adams and A. McMechen of Lockheed-Martin Astronautics Co. for their technical expertise; J. Bevan for computer software support; J. Twicken and D. Hinson of Stanford University for providing the MGS Radio Science USO data; T. Priest and the MGS Navigation Team for providing trajectory files; the DSS-13 station personnel for conducting the experiments (G. Bury, J. Crook, G. Farner, J. Garnica, R. Littlefair, R. Reese, and L. Smith); L. Teitelbaum, and P. Wolken for scheduling support; and M. Speranza, T. Buckley, L. Moreno, and A. Milanian for assistance in data processing.

8. REFERENCES

[1] D. Morabito, S. Butman, and S. Shambayati "The Mars Global Surveyor Ka-band Link Experiment (MGS/KaBLE-II)", The Telecommunications and Data Acquisition Progress Report 42-137, January-March 1999, Jet Propulsion Laboratory, Pasadena, California, May 15, 1999.

[2] S. Butman, et. al. "The Mars Global Surveyor Ka-band Link Experiment (MGS/KaBLE-II)", in the proceedings of the 3rd Ka-band Utilization Conference, November. 1997, held in Sorrento, Italy.

[3] D. Morabito, S. Butman, and S. Shambayati "Recent Results from the Mars Global Surveyor Ka-band Link Experiment (MGS/KaBLE-II)", in the proceedings of the 4th Ka-band Utilization Conference, November. 1998, held in Venice, Italy.

[4] D. Morabito and S. W. Asmar "Radio Science Performance Analysis Software", The Telecommunications and Data Acquisition Progress Report 42-120, vol. October-December 1994, Jet Propulsion Laboratory, Pasadena, California, February 15, 1995, pp. 121-152.

[5] Armstrong, J. W., Woo, R. and Estabrook, F. B., "Interplanetary Phase Scintillation and the Search for Very Low frequency Gravitational Radiation", The Astrophysical Journal, **230**, 570-574, June 1, 1979.

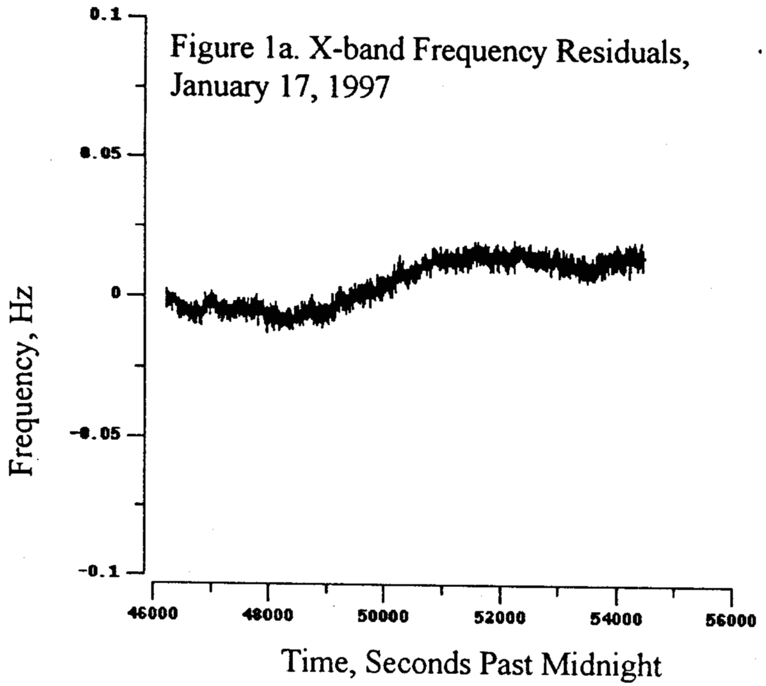

Figure 1a. X-band Frequency Residuals, January 17, 1997

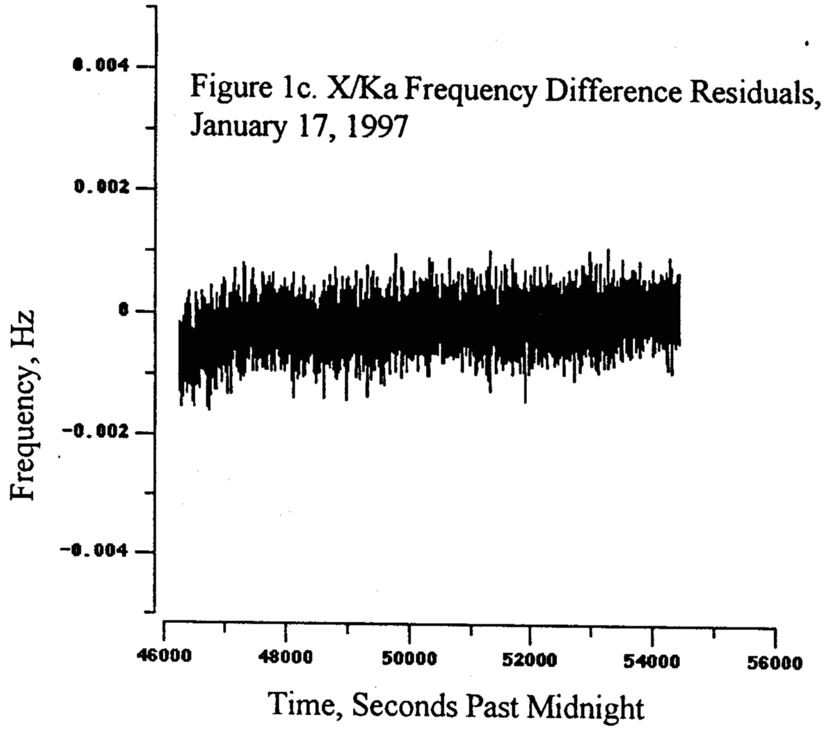

Figure 1c. X/Ka Frequency Difference Residuals, January 17, 1997

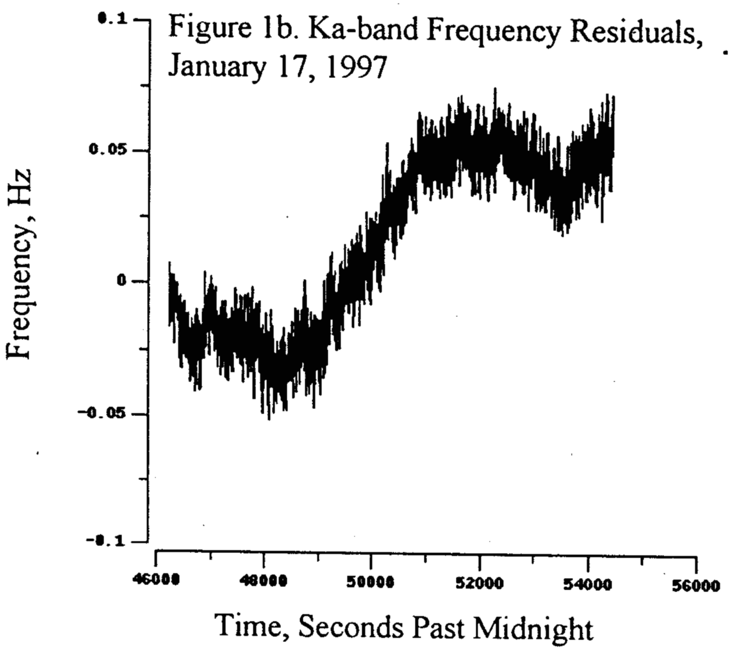

Figure 1b. Ka-band Frequency Residuals, January 17, 1997

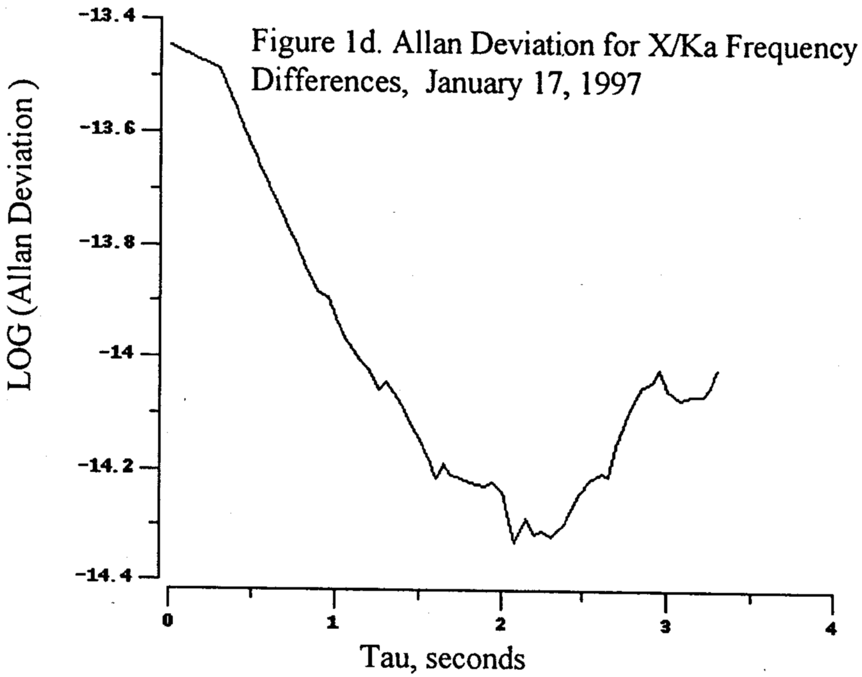

Figure 1d. Allan Deviation for X/Ka Frequency Differences, January 17, 1997

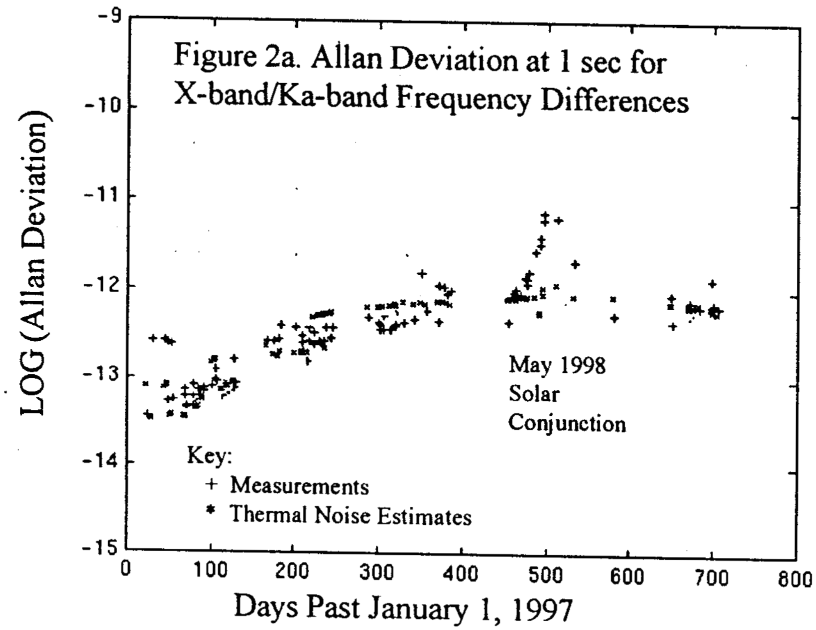
Figure 2a. Allan Deviation at 1 sec for
X-band/Ka-band Frequency Differences
May 1998
Solar
Conjunction
Key:
+ Measurements
* Thermal Noise Estimates
LOG (Allan Deviation)
Days Past January 1, 1997
-9
-10
-11
-12
-13
-14
-15
0
100
200
300
400
500
600
700
800

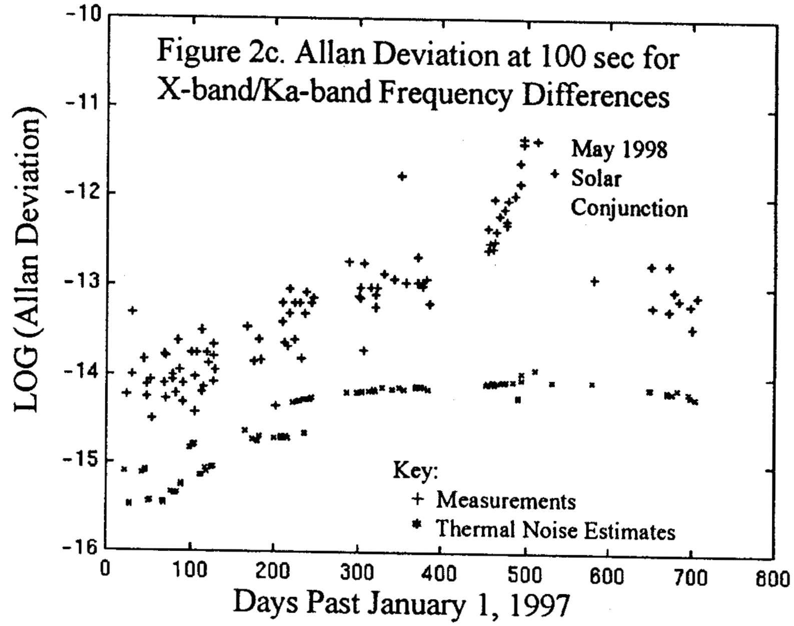
Figure 2c. Allan Deviation at 100 sec for
X-band/Ka-band Frequency Differences
May 1998
Solar
Conjunction
Key:
+ Measurements
* Thermal Noise Estimates
LOG (Allan Deviation)
Days Past January 1, 1997
-10
-11
-12
-13
-14
-15
-16
0
100
200
300
400
500
600
700
800

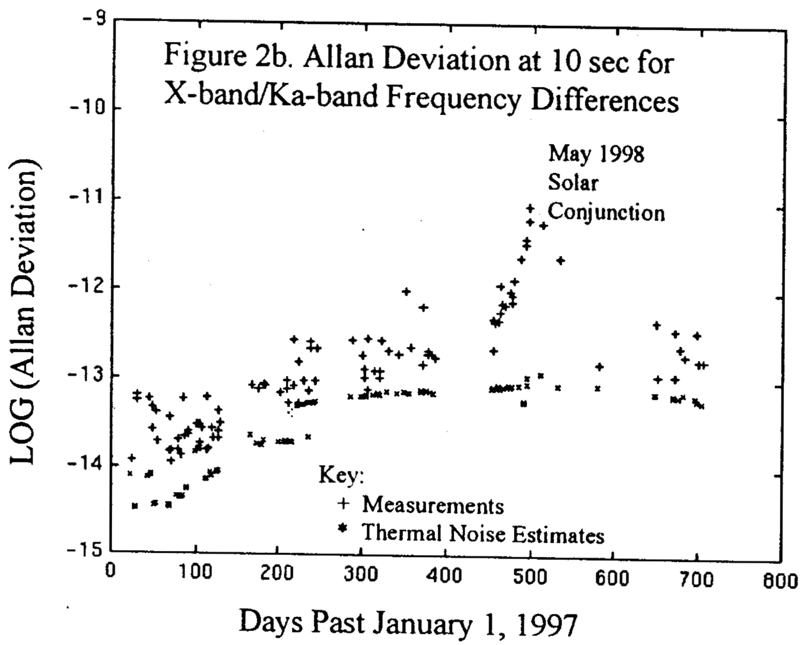
Figure 2b. Allan Deviation at 10 sec for
X-band/Ka-band Frequency Differences
May 1998
Solar
Conjunction
Key:
+ Measurements
* Thermal Noise Estimates
LOG (Allan Deviation)
Days Past January 1, 1997
-9
-10
-11
-12
-13
-14
-15
0
100
200
300
400
500
600
700
800

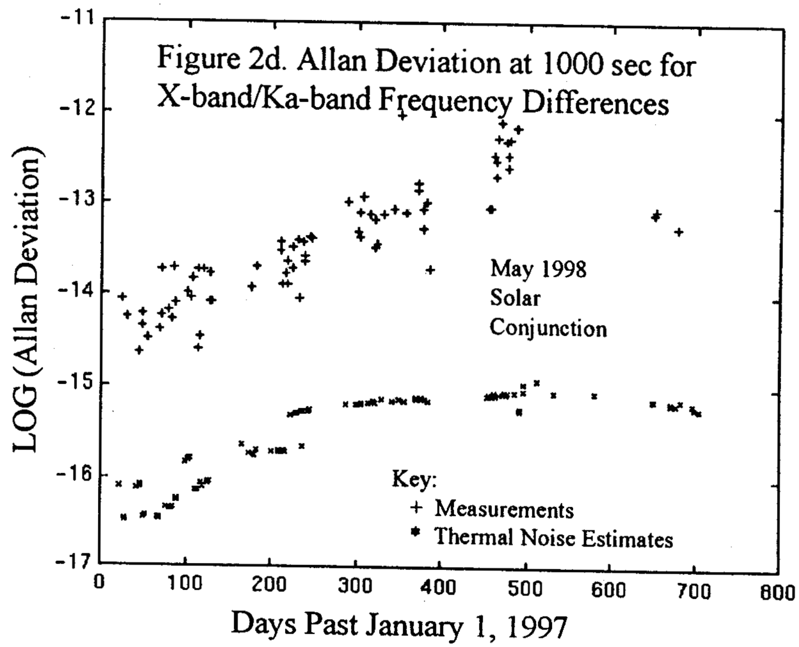
Figure 2d. Allan Deviation at 1000 sec for
X-band/Ka-band Frequency Differences
May 1998
Solar
Conjunction
Key:
+ Measurements
* Thermal Noise Estimates
LOG (Allan Deviation)
Days Past January 1, 1997
-11
-12
-13
-14
-15
-16
-17
0
100
200
300
400
500
600
700
800

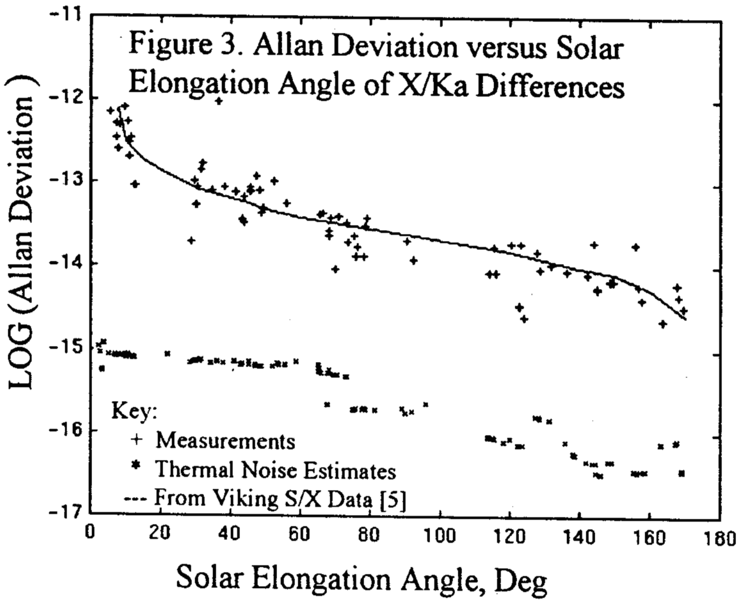

Figure 3. Allan Deviation versus Solar Elongation Angle of X/Ka Differences

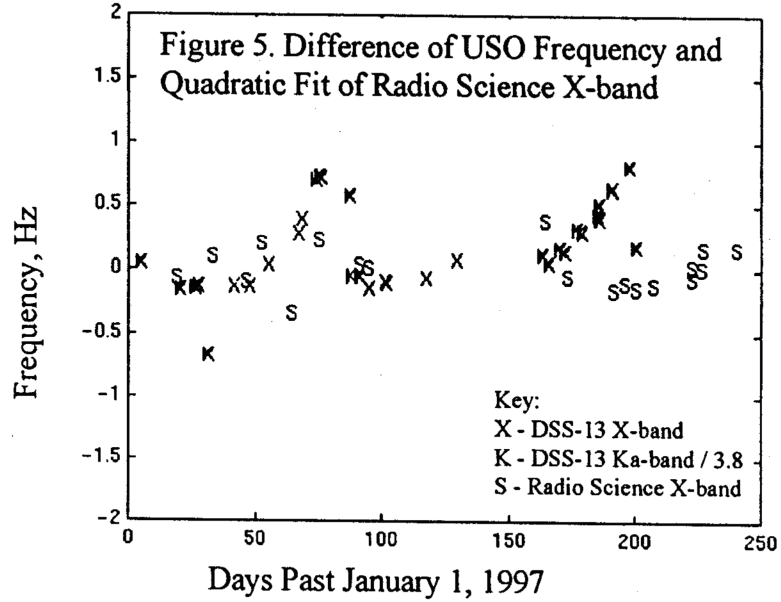

Figure 5. Difference of USO Frequency and Quadratic Fit of Radio Science X-band

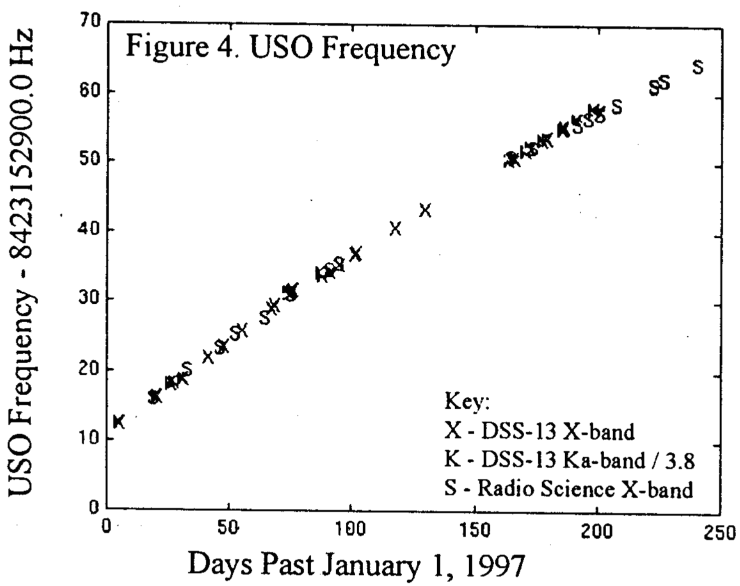

Figure 4. USO Frequency

Figure 6. Difference of DSS-13 X-band and Ka-band USO Frequencies